

Ultraviolet photodissociation dynamics of formyl fluoride

Part 2† Energy disposal in the H + FCO product channel

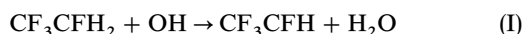
Claire L. Reed, Mitsuhiro Kono,‡ Stephen R. Langford, Richard N. Dixon and Michael N. R. Ashfold*§

School of Chemistry, University of Bristol, Bristol, UK BS8 1TS

The technique of H (Rydberg) atom photofragment translational spectroscopy has been used to investigate the total kinetic energy release (TKER) into the H + FCO fragments resulting from near UV photolysis of jet-cooled formyl fluoride, HC(O)F, molecules at numerous wavelengths in the range 248.2–218.4 nm. Analysis of the TKER spectra yield a precise value for the C–H bond dissociation energy $D_0[\text{H}-\text{C}(\text{O})\text{F}] = 34950 \pm 20 \text{ cm}^{-1}$, and allow an estimate of the height of the energy barrier in the alternative, and previously unobserved, C–F bond fission channel. Photolysis at the longest wavelengths within this range results in FCO(\tilde{X}) products carrying only modest rotational and vibrational excitation (the former concentrated in the form of *a*-axis rotation); the bulk of the available energy $\{i.e., E_{\text{phot}} - D_0[\text{H}-\text{C}(\text{O})\text{F}]\}$ appears as product translation. The rotational energy disposal is deduced to be almost invariant to excitation wavelength, but the extent of product vibration is found to increase near linearly with increasing E_{phot} . These observations are all explicable in terms of a fragmentation mechanism in which the photo-excited HC(O)F(\tilde{A}) molecules undergo intersystem crossing (ISC) to the neighbouring $\tilde{a}^3\text{A}'$ surface and then evolve over (or through) an energy barrier in the H–C(O)F dissociation coordinate. A simple impact parameter model suffices to show that the rotational energy disposal is determined largely by the geometry and the forces acting as the molecule traverses this barrier region. The observed energy partitioning between FCO vibration and product recoil is explained in terms of a statistical fragmentation process occurring above a potential-energy barrier. The available energy, E_{avl} , is viewed in terms of two energy reservoirs: the first of these, corresponding to the exit channel barrier itself, is released impulsively (mainly into product translation), whilst the other, containing the remainder of E_{avl} , is partitioned statistically amongst the various energetically accessible vibrational states of the FCO fragment. H atom tunnelling is explicitly incorporated in the model and serves to blur the sub-division between these two energy reservoirs. Its inclusion allows good replication of all measured TKER spectra within the range of photolysis wavelengths investigated.

Introduction

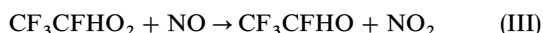
Formyl fluoride [HC(O)F] has been identified as a major degradation product of HFC-134a¹ (CF₃CFH₂), a proposed CFC replacement for use in automobile air-conditioning and domestic refrigeration. HFC-134a is not expected to affect the concentration of stratospheric ozone^{2,3} and has a limited global warming potential.⁴ The atmospheric degradation of HFCs is initiated by OH radical attack, *i.e.* in the case of HFC-134a



followed by conversion to a peroxy radical by reaction with oxygen, *viz.*

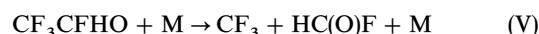
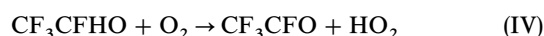


The peroxy radical formed can then react rapidly with NO to give the alkoxy radical CF₃CFHO:^{5–7}



In order to gain a complete picture of the degradation of HFC-134a it is necessary to examine all the decomposition pathways. A major question relates to the fate of the alkoxy

radical, which can either react with O₂ or decompose



Since CF₃CFO is readily hydrolysed to form CF₃COOH^{8–10} (trifluoroacetic acid, TFA), a somewhat phytotoxic compound,^{8,11,12} the branching ratios between reactions (IV) and (V) are of significant interest.^{13–15} Formyl fluoride is proposed to be of no importance in ozone depleting catalysis cycles,³ however, its stratospheric lifetime and rates of photolysis have not yet been measured (they are predicted to be similar to F₂CO, which has a lifetime of less than 0.6 years at 25 km²). It is therefore important that the stratospheric dissociation of HC(O)F be considered. The remainder of this paper focuses on the primary photochemistry of HC(O)F at near-UV wavelengths applicable to the stratosphere and attempts to place the results in context with current theories of this molecule.

The planar equilibrium geometry of the ground state of formyl fluoride (*C_s* symmetry) has been confirmed by IR¹⁶ and microwave^{17,18} studies. The structured electronic absorption in the region 267–220 nm, associated with the $\tilde{A}^1\text{A}' \leftarrow \tilde{X}^1\text{A}'$ transition, is dominated by a progression in the excited state CO stretching mode (ν_2) as expected given that it arises as a result of an $\pi^* \leftarrow n$ electron promotion centred on the C=O moiety.^{19,20} The early analyses^{19,20} established the band origin (37 491.7 cm⁻¹), the extended CO bond length in the \tilde{A} state and also showed this state to be non-planar, with an out-of-plane angle of 30–35° with respect to the FCO plane.

† For Part 1 see ref. 32.

‡ Present address: Department of Pure and Applied Sciences, College of Arts and Sciences, University of Tokyo, Komaba, Meguro-Ku, Tokyo, 153 Japan.

§ E-mail: mike.ashfold@bristol.ac.uk

Assignments of the pattern of \tilde{A} state vibrational levels have been extended and refined by Fischer²¹ and, latterly, by Crane *et al.*²² using data from jet-cooled LIF spectra²³ and *ab initio* calculations.²⁴

Studies on the dissociation of HC(O)F molecules following their excitation to the \tilde{A}^1A'' state have been scarce. Klimek and Berry²⁵ found that the HF products resulting from (broad band) UV excitation of HC(O)F molecules had an inverted vibrational population distribution, but that HF vibration still accounted for only *ca.* 7% of the available energy. Weiner and Rosenfeld²⁶ used kinetic absorption spectroscopy to measure the CO formation rate following photoexcitation at 248 and 193 nm, and concluded that the simple bond fission channels H + FCO and/or F + HCO were the major dissociation pathways at these wavelengths, with some evidence for formation of H + F + CO products at 193 nm. A theoretical calculation by Sumathi and Chandra²⁷ predicted H + FCO to be the most probable dissociation products for HC(O)F molecules following their excitation to the \tilde{A} state, but also indicated the presence of a potential barrier of *ca.* 14 000 cm⁻¹ from the transition state to the ground state products; more recent calculations²⁸ suggest that this barrier height is closer to 7000 cm⁻¹. Such fragmentation behaviour is in direct contrast to that deduced for ground state HC(O)F molecules, which show a marked preference for dissociation to the molecular products HF + CO. Choi and Moore^{29–31} have performed detailed state-specific experiments on this molecular elimination channel from highly vibrationally excited ground state molecules (prepared by stimulated emission pumping from known \tilde{A} state levels), thereby determining an activation energy of 176 kJ mol⁻¹ (14 750 cm⁻¹) measured from the \tilde{X} state origin for molecules dissociating *via* this pathway.

This paper is concerned with the radical dissociation channel



and extends recent studies of this same channel reported in Part 1.³² Comparisons of the jet-cooled parent \tilde{A} – \tilde{X} laser induced fluorescence (LIF) spectrum and the ‘action’ spectrum for forming H atom photoproducts have yielded a value of *ca.* 39 690 cm⁻¹ as the appearance threshold for forming H atoms.^{32,33} Analyses of the Doppler lineshape of these H atom fragments suggests that *ca.* 5000 cm⁻¹ is released as recoil energy, even at energies close to this appearance threshold. Measurements of the recoil anisotropy³⁴ also point to the fact that dissociation proceeds *via* intersystem crossing (ISC) to the (as yet unobserved) triplet (\tilde{a}^3A'') state at non-planar geometries and that there is a barrier in the C–H dissociation co-ordinate on this triplet potential-energy surface. Such conclusions are broadly consistent with the *ab initio* predictions^{27,28} regarding the geometry and nature of the excited-state potential-energy surfaces.

In this study H (Rydberg) atom photofragment translational spectroscopy (PTS)³⁵ has been employed to study the detailed dynamics of the dissociation channel in reaction (VI) following excitation of jet-cooled HC(O)F molecules at numerous wavelengths in the range from 248.2 nm (40 280 cm⁻¹, an energy just above the H atom appearance threshold) to 218.4 nm (45 735 cm⁻¹). In a previous work³⁶ we reported preliminary results obtained at the longest excitation wavelengths that serve to define the bond dissociation energy (D_0) for channel (VI) as $34\,950 \pm 20$ cm⁻¹ and confirm that the bulk of the photolysis energy in excess of that required for C–H bond fission (E_{av}) is released in the form of H + FCO product translation, with the residue partitioned largely into *a*-axis rotation of the FCO fragment. Here we show that decreasing excitation wavelength (*i.e.* increasing excitation energy) results in a near monotonic increase in the extent of FCO product internal (mainly vibrational) excitation, but has little effect on the product rotational energy disposal. The

observed energy disposal is explained and reproduced, qualitatively, in terms of a hybrid model, including tunnelling, in which the energy associated with the exit channel barrier is partitioned dynamically whilst the remainder of E_{av} is partitioned statistically over the available vibrational states of the FCO product.

Experimental

The H atom PTS technique has been described previously.^{35,37–39} Formyl fluoride was generated by the reaction between cyanuric fluoride and formic acid according to the method of Olah *et al.*⁴⁰ A molecular beam of formyl fluoride was prepared by passing *ca.* 1 atm of Ar (or N₂) over a sample of liquid HC(O)F stored at dry-ice temperature and introduced into the experiment *via* a pulsed nozzle (General Valve Series 9) mounted in its own diffusion pumped chamber and thence, *via* a skimmer, into the cryopumped reaction chamber. The HC(O)F molecules are photolysed by one laser pulse (in the wavelength range 248.2–218.4 nm), which intercepts the molecular beam at right angles downstream from the skimmer, and the resulting H atoms are then ‘tagged’ using two laser pulses (which counter-propagate with respect to the photolysis laser pulse) to effect two-photon resonant excitation to a high-*n* Rydberg state. The photolysis wavelengths used were provided by a Nd-YAG pumped dye laser (Spectra-Physics GCR-270 plus PDL 2) operating on the dyes Coumarin 440, 460, 480 and 500 with subsequent doubling of the dye laser output in BBO. The H atoms fly a field-free distance of 425 mm along the axis orthogonal to the molecular beam and the laser beams and are field ionised immediately prior to detection by a Johnston multiplier (type MM1-SG). The output from the multiplier is amplified and sent to one channel of a digital storage oscilloscope (LeCroy 9450, 350 MHz bandwidth) for display. The transient time-of-flight (TOF) spectrum so obtained is then transferred to a computer (IBM PS-2) *via* a GPIB interface and the spectrum accumulated over typically 10⁴ laser shots. Energy and momentum conservation allows conversion of the TOF spectra into total kinetic energy release (TKER) spectra.^{35,37–39}

Results

The observable in these experiments is a spectrum of H atom yield as a function of time, t_{H} , after the laser photolysis pulse. Fig. 1 shows H atom TOF spectra obtained following linearly polarised photolysis (ϵ perpendicular to the TOF axis) of jet-cooled HC(O)F molecules at (a) 218.4 nm and (b) 232.9 nm. We begin by considering just the latter peak in (a) and the only peak in (b) both of which, as we now show, are associated with the primary one-photon dissociation of HC(O)F. We return to consider the origins of the earlier peak in (a) later. The $t_{\text{H}} > 25$ μs part of these TOF spectra can be converted to TKER spectra *via* the relationship:

$$\text{TKER} = \text{KE}_{\text{H}} + \text{KE}_{\text{FCO}} = \frac{1}{2} m_{\text{H}} \left\{ 1 + \frac{m_{\text{H}}}{m_{\text{FCO}}} \right\} \left(\frac{d}{t_{\text{H}}} \right)^2 \quad (1)$$

where d is the flight distance (425 mm), KE_{H} and KE_{FCO} are the respective fragment kinetic energies and m_{H} and m_{FCO} are the corresponding masses. Fig. 2 shows a representative set of TKER spectra for the H + FCO(\tilde{X}) fragments resulting from HC(O)F photolysis at four different excitation wavelengths. All spectra recorded in this work reveal fine structure, which, after careful analysis, can provide an insight into the energy disposal within the FCO radical. Note the very similar fall off in signal intensity at low TKER in the spectra obtained at each of these four wavelengths, and in all other TKER spectra obtained in this study.

These TKER spectra are transformed into spectra of the FCO fragment internal energy, E_{int} , using the relationship

$$E_{\text{int}} = E_{\text{phot}} - D_0[\text{H-C(O)F}] - \text{TKER} \quad (2)$$

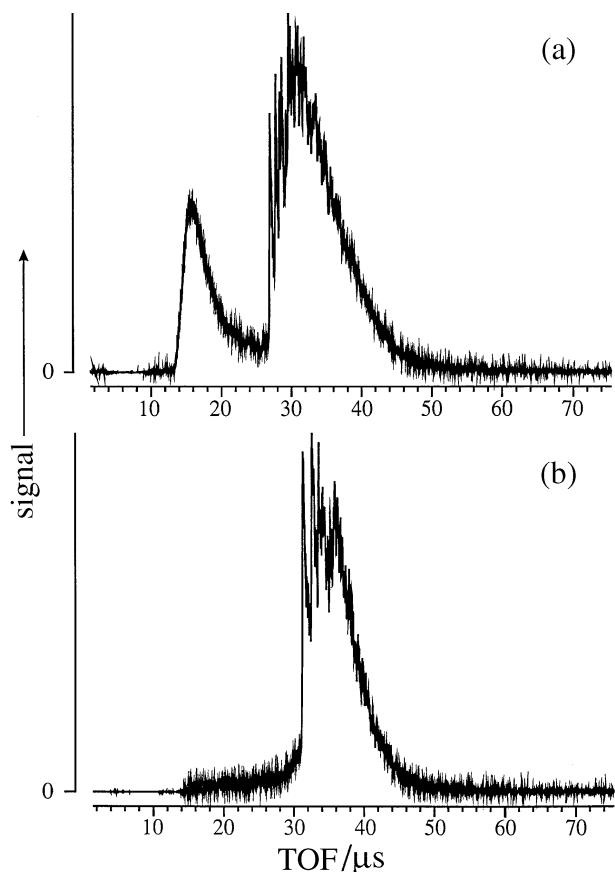


Fig. 1 H (Rydberg) atom TOF spectra obtained following linearly polarised photolysis of a jet-cooled sample of HC(O)F molecules at (a) 218.4 nm and (b) 232.9 nm. The peak appearing at *ca.* 30 μ s in both spectra is due to H atoms arising *via* the C–H bond fission channel (VI), whilst the earlier peak evident in (a) is attributed to secondary photolysis of HCO(\tilde{X}) fragments arising *via* the alternative C–F bond fission (VII).

where E_{phot} is the photolysis photon energy, $D_0[\text{H–C(O)F}] = 34\,950 \pm 20 \text{ cm}^{-1}$ ³⁶ and we neglect the (small) residual internal energy in the jet-cooled parent molecules. Fig. 3 shows three illustrative examples of such spectra, together with

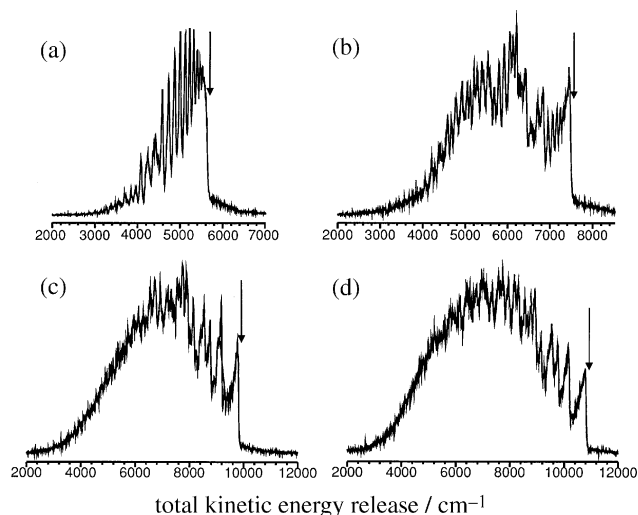


Fig. 2 TKER spectrum of the H + FCO(\tilde{X}) fragments resulting from linearly polarised photolysis (ϵ perpendicular to the TOF axis) of a jet-cooled sample of HC(O)F molecules at (a) 246.3 nm ($40\,590 \text{ cm}^{-1}$), (b) 235.66 nm ($42\,420 \text{ cm}^{-1}$), (c) 223.34 nm ($44\,760 \text{ cm}^{-1}$) and (d) 218.4 nm ($45\,775 \text{ cm}^{-1}$). The vertical arrow in each spectrum indicates the deduced TKER_{max} , *i.e.* the TKER associated with formation of FCO fragments in their $v = N = 0$ level, from which we deduce $D_0[\text{H–C(O)F}] = 34\,950 \pm 20 \text{ cm}^{-1}$.

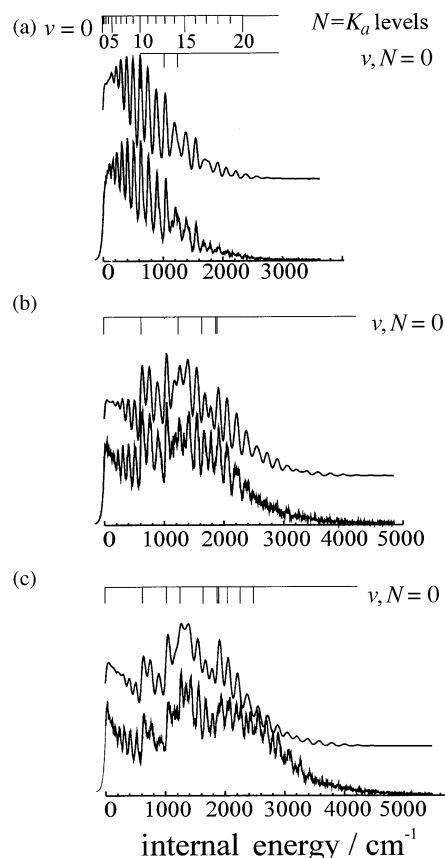


Fig. 3 Internal energy spectra of the FCO fragments resulting from photolysis of jet-cooled HC(O)F molecules at (a) 246.3 nm ($40\,590 \text{ cm}^{-1}$), (b) 239.2 nm ($41\,800 \text{ cm}^{-1}$) and (c) 235.66 nm ($42\,420 \text{ cm}^{-1}$). The upper trace in each panel shows the best-fit simulation of each spectrum obtained assuming population of just those rotational states with $N = K_a$, a Gaussian distribution over these states as described by eqn. (4) with $K_{a(\text{max})} = 8$ and $\Delta K_a = 9$ for (a) or $\Delta K_a = 10$ for (b) and (c), the following relative vibrational state populations: (a) 0_0 (78%), 3_1 (12%), 2_1 (8%), 3_2 (2%); (b) 0_0 (35%), 3_1 (21%), 2_1 (15%), 3_2 (16%), $2_1 3_1$ (5%), 1_1 (3%), 3_3 (5%); (c) 0_0 (25%), 3_1 (12%), 2_1 (15%), 3_2 (16%), $2_1 3_1$ (4%), 1_1 (7%), 3_3 (4%), 2_2 (7%), $2_1 3_2$ (5%), 3_4 (7%) and a quantum state width of 90 cm^{-1} (FWHM, Gaussian). The comb across the top of the figure indicates the energies of the various $N = K_a$ levels associated with the $v = 0$ vibrational state, whilst the additional comb festooned over each spectrum indicates the energies of the rotationless level associated with all of the vibrational states included in each fit.

assignments of many of the more prominent features. The fundamental vibrational frequencies of FCO(\tilde{X}) are known,^{41,42} and listed in Table 1. From these parameters, it is possible to estimate (in the harmonic limit) the energies of the various overtone and combination levels of FCO(\tilde{X}) and thus begin assigning the various fragment internal energy spectra. In this we are also guided by the previous vibronic analysis of the low resolution electronic emission spectrum of the FCO radical reported by Toby and Toby⁴³ but, clearly, assignment

Table 1 Normal-mode vibrational frequencies of FCO(\tilde{X}) and selected rotational constants for the ground vibrational state of FCO(\tilde{X})^{41,42}

parameter	wavenumber/ cm^{-1}
ν_1 (CO stretch)	1861
ν_2 (CF stretch)	1026
ν_3 (FCO bend ^a)	626
A	6.3778
B	0.382
C	0.360
ΔK	1.318×10^{-3}

^a Determined only in a matrix.⁴²

of individual features in these spectra becomes progressively less certain as the internal energy increases.

FCO is a near prolate symmetric top. Thus its pattern of rotational energy (E_{rot}) levels exhibits coarse K structure (associated with a -axis rotation), each with a stack of N levels ($N \geq K_a$) extending to higher energies. The rotational contribution to the total energy was calculated using the expression

$$E_{\text{rot}} = \bar{B}N(N + 1) + (A - \bar{B})K_a^2 - \Delta_K K_a^4 \quad (3)$$

where $\bar{B} = (B + C)/2$ and A , B and C are the rotational constants⁴¹ and (given the experimental resolution) only the centrifugal term involving K_a^4 (Δ_K) is included. Given the width and symmetry of the resolved peaks, particularly those in the spectra taken at the longer excitation wavelengths, it is clear that the fragmentation process has a propensity for forming FCO fragments with $N \approx K_a$ (i.e. with virtually all of the fragment angular momentum concentrated in the form of a -axis rotation). Rotational levels associated with the $v_3 = 1$ state are sufficiently well resolved in the TKER spectra obtained at longer excitation wavelengths (e.g. 246.3 nm) that it is possible to assess the effect of bending excitation upon the A rotational constant. The best simulations of the $v_3 = 1$ structure require A to be increased to 6.569 cm^{-1} (a 3% increase relative to that for the $v = 0$ level), reflecting the asymmetry of the bending potential about its minimum. Our later simulations assume a further 3% increase in A for each additional quantum of bending excitation.

The rotational quantum state population distribution, $P(K_a)$, and thus the intensity distribution, $I(K_a)$, is most easily determined³⁶ for the least overlapped $v = 0$ product state and found to be reproduced well by a Gaussian function spanning just the $N = K_a$ levels

$$I(K_a) \propto \exp\left\{\frac{-4 \ln 2 [K_a - K_{a(\text{max})}]^2}{(\Delta K_a)^2}\right\} \quad (4)$$

with the most populated level, $K_{a(\text{max})} = 8$ and a full width half maximum (FWHM) (ΔK_a) that varies from 9 at the longest excitation wavelengths to ca. 11 at the shortest wavelengths. Careful scrutiny of the spectra taken at the longer excitation wavelengths failed to reveal any indications that the rotational energy disposal depended upon the particular vibrational state in which the product was formed. Thus, for any given TKER spectrum, $I(K_a)$ was assumed to be independent of v . The simulations shown in Fig. 3 were obtained assuming a rotational state distribution for each populated vibrational level as defined in eqn. (4) and least-squares fitting to the observed spectra whilst floating the following parameters: $K_{a(\text{max})}$ and ΔK_a (defining the distribution over the $N = K_a$ states), the half width half height of the peak associated with any individual quantum state (in cm^{-1} , and assumed Gaussian), and the relative population of each vibrational state. Such a procedure allows detailed simulation of the fragment internal energy spectra obtained at all excitation wavelengths down to ca. 235 nm ($E_{\text{av1}} = E_{\text{phot}} - D_0[\text{H-C(O)F}] \approx 7600 \text{ cm}^{-1}$). The FCO fragments that result from photolysis at shorter wavelengths carry a yet broader spread of internal energies. Simulation of the low E_{int} ($\leq \text{ca. } 2500 \text{ cm}^{-1}$) part of these spectra remains straightforward, but the lack of precise vibrational term values for the higher vibrational levels of FCO and the general increase in product vibrational state density hinders unambiguous interpretation of the higher energy part of the observed spectra. For these shorter excitation wavelengths we therefore choose, instead, just to quote a value for $\langle E_{\text{int}} \rangle$, the average internal energy content of the FCO fragments.

Fig. 4 shows that $\langle E_{\text{int}} \rangle$ increases roughly monotonically with increasing E_{av1} , with a slope of ca. 0.6, and showing some hint of undulatory structure. The intercept (at $E_{\text{av1}} \approx 4900 \text{ cm}^{-1}$) accords well with the previously reported difference

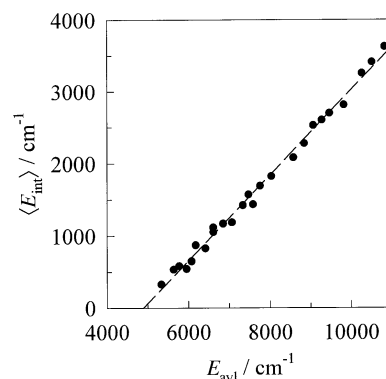


Fig. 4 Plot showing the linear correlation between $\langle E_{\text{int}} \rangle$ and E_{av1} ($= E_{\text{phot}} - D_0[\text{H-C(O)F}]$), together with the best-fit straight line (with gradient 0.6). The intercept at $\langle E_{\text{int}} \rangle = 0 \text{ cm}^{-1}$ corresponds to the threshold observed for forming H atoms, ca. 4900 cm^{-1} . The uncertainties in $\langle E_{\text{int}} \rangle$ are estimated as being of similar magnitude to the size of the data points in the plot.

between $D_0[\text{H-C(O)F}]$ and the observed threshold energy for forming H atom photoproducts [dissociation channel (VI)].³⁶ At the longer excitation wavelengths, close to this threshold, we observe that the bulk of E_{av1} is channelled into translational excitation of the products, with but modest amounts of a -axis rotational excitation and little vibrational excitation of the FCO product. As the photolysis wavelength is reduced (i.e. E_{av1} is increased), both $\langle E_{\text{int}} \rangle$ and the fraction of the total E_{av1} partitioned into product internal excitation increases. The spectral simulations show the extent of product rotation to be essentially independent of excitation wavelength (within the wavelength range studied), thus the increase in $\langle E_{\text{int}} \rangle$ is entirely attributable to an increase in product vibration. In what follows, we present a detailed rationale for this observed pattern of energy disposal.

Before concluding this section we return to consider the faster peak evident in the TOF spectrum recorded at 218.4 nm [Fig. 1(a)]. A comparable feature appears, but with progressively decreasing intensity, in all H atom TOF spectra recorded at wavelengths as long as 232.9 nm. We consider two possible explanations for this peak. The parent 'action' spectrum for forming H atoms shows resolved rovibronic structure,^{32,34} indicating that even this far above its electronic origin the \tilde{A} state of HC(O)F has a finite (probably picosecond) lifetime with respect to fragmentation. Thus one possible explanation for such fast H atoms in the TOF spectrum could be two-photon excitation of HC(O)F, resonance enhanced at the one photon energy, and subsequent dissociation to yield $\text{H} + \text{FCO}(\tilde{X})$ fragments with a broad spread of internal energies. The lack of any 'fast' signal at longer excitation wavelengths could be attributed to a lack of any suitable excited state for the second one-photon absorption step, but such seems unlikely given the expected electronic state density at such high energies. The alternative, and our preferred, explanation is that these fast H atoms are associated with secondary photolysis of $\text{HCO}(\tilde{X})$ fragments resulting from the alternative C-F bond fission channel



which is calculated to be exoergic at excitation energies above ca. 31 500 cm^{-1} .³⁶ The $\tilde{B}-\tilde{X}$ and $\tilde{C}-\tilde{X}$ systems of HCO have origins at 38 691 cm^{-1} and 41 270 cm^{-1} , respectively⁴⁴ and given the geometry changes that accompany these electronic excitations, we can anticipate absorption due to this radical throughout the wavelength range of the present study. We comment that an entirely analogous fast peak is observed⁴⁵ in the TOF spectrum of the H atoms arising in the near-UV photolysis of the isoelectronic species HCOOH, at wavelengths where dissociation to the fragments $\text{OH} + \text{HCO}$ is

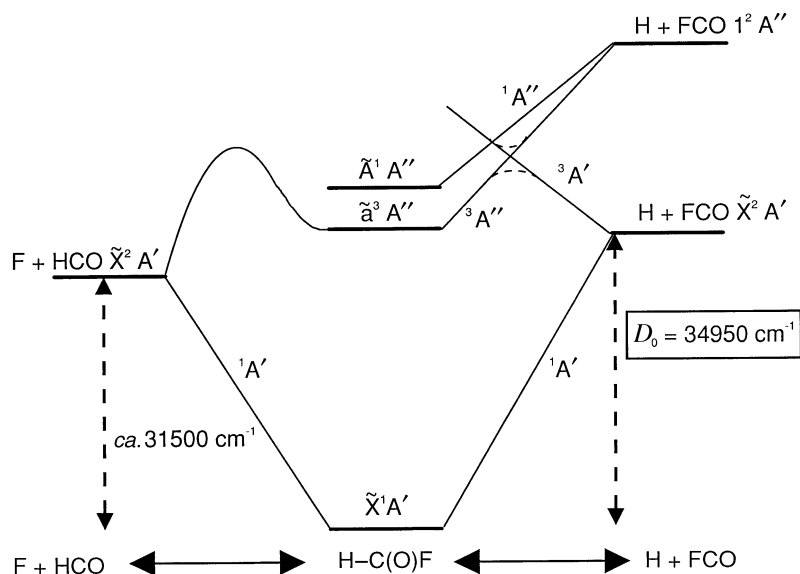


Fig. 5 Schematic correlation diagram for the fragmentation of HC(O)F *via* C–H and C–F bond fission. The solid lines show the parent–product correlations appropriate for planar geometries (C_s point group), whilst the dashed lines indicate the avoided crossings between the triplet surfaces that apply under the reduced (C_1) symmetry appropriate for non-planar configurations. The crossing of the $^3A''$ and $^3A'$ surfaces at planar geometries gives rise to a conical intersection with respect to the out-of-plane bending motion in each exit channel.

known to be the dominant process,^{46,47} but reserve further discussion of the significance of these observations *vis à vis* the energetics of process (VII) until later.

Discussion

I Potential-energy surfaces of HFCO and rotational-energy disposal in the FCO fragment

Any discussion of the photodissociation dynamics of formyl fluoride must start with a consideration of relevant portions of the potential-energy surfaces for HC(O)F molecules in their ground and first two excited electronic states (the \tilde{A}^1A' and \tilde{a}^3A'' states, both arising from an $\pi^* \leftarrow n$ electron promotion centred on the C=O group). Symmetry arguments,³⁴ summarised in Fig. 5, suggest that the ground state of HC(O)F correlates with the ground state products H + FCO(\tilde{X}^2A'), whilst the photoexcited HC(O)F(\tilde{A}) molecules must correlate adiabatically with the lowest energy excited products of A'' symmetry. *Ab initio* calculations^{48,49} show these to be the products H + FCO($1^2A''$), with this valence excited state of the radical lying *ca.* 25 000 cm^{-1} above the \tilde{X}^2A' ground state. Not surprisingly, we see no evidence for this higher energy product channel even at the shortest excitation wavelengths studied in this work. As discussed in the Introduction, it is possible to envisage two possible routes to the ground state FCO(\tilde{X}) products we identify following photoexcitation to the \tilde{A} state of formyl fluoride. Crane *et al.*²² have clearly shown the importance of internal conversion (IC) to the ground state surface at excitation energies below the threshold for the H + FCO(\tilde{X}) radical channel, and studies from Choi and Moore^{29,31} indicate that molecular elimination to the products HF + CO is dominant at these energies. IC is unlikely to provide the route from \tilde{A} state parent molecules to the ground state radical products (VI), however. Experiment^{34,36} points to the presence of an energy barrier somewhere in the exit channel leading from the parent \tilde{A} state to the H + FCO(\tilde{X}) products, but neither correlation arguments³⁴ nor *ab initio* calculations^{24,27} indicate any significant barrier in the C–H dissociation co-ordinate of the ground-state surface.

ISC to the \tilde{a}^3A'' surface represents an alternative possible fragmentation route for \tilde{A} state parent molecules, and all recent studies^{32–34,36} suggest that this is the initial step in the radical dissociation channel (VI). As Fig. 5 shows, the C–H

exit channel of the triplet surface supports the bottom half of a conical intersection. The magnitude of the associated energy barrier decreases with increasing out-of-plane bending angle, but is calculated^{27,28} to be very significant still at the transition state to fragmentation *via* C–H bond fission. The transition state (*i.e.* the saddle-point corresponding to the top of the barrier in the C–H dissociation co-ordinate) is pyramidal,²⁸ as shown in Fig. 6, with an extended C–H bond length (1.53 Å) and an out-of-plane angle of 75° measured relative to the plane defined by the FCO partner fragment. (For reference, the corresponding values at the equilibrium geometry of the \tilde{a}^3A'' state are calculated to be 1.10 Å and *ca.* 52°.²⁸) If fragmentation simply involved further extension of the C–H bond along this axis, the impact parameter, b , associated with this trajectory (relative to the FCO centre of mass) would be 0.43 Å. As shown previously,³⁶ this is in close accord with the value (*ca.* 0.47 Å) obtained *via* the relationship

$$K_{a(\text{max})} \hbar = \mu v b \quad (5)$$

with $K_{a(\text{max})} \approx 8$ (derived experimentally), ($\mu = 0.987$ u for an H atom recoiling from FCO, and a recoil velocity, $v \approx 11\,000$ m s^{-1} , appropriate for the longest photolysis wavelengths used in this study.

Hence we arrive at a reasonably detailed picture of the rotational energy disposal accompanying this dissociation process, at least near its long wavelength appearance threshold; Franck–Condon considerations dictate that the HC(O)F(\tilde{A}) molecules will be created with substantial out-of-plane vibrational motion. These \tilde{A} state molecules have a finite lifetime (as evidenced by the structured appearance of the parent \tilde{A} – \tilde{X} absorption spectrum^{32,33}) but at some later instant undergo a prompt electronic rearrangement and access the \tilde{a}^3A'' surface. C–H bond extension then carries these molecules into the

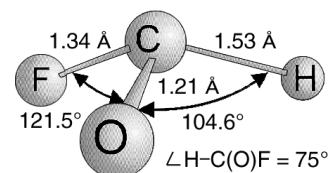


Fig. 6 Calculated²⁸ geometry of HC(O)F molecules at the transition state (*i.e.* the saddle-point associated with the minimum energy pathway over the barrier) in the H–C(O)F exit channel of the \tilde{a}^3A'' potential-energy surface

confined region of phase space associated with the energy barrier in this exit channel. The observed proclivity for fragment *a*-axis rotation, and the extent of this rotational excitation, is broadly consistent with that predicted on the basis of a simple impact parameter model in which the impulse is 'switched on' at the transition state, and the departing H atom recoils along an axis that is nearly perpendicular to the FCO plane.

Finally in this Section we return to consider the alternative C—F bond fission channel (VII). Having determined $D_0[\text{H—C(O)F}]$, and taking literature values for $\Delta_r H^\circ(\text{H})$, $\Delta_r H^\circ(\text{F})$, $\Delta_r H^\circ(\text{HCO})$ ⁵⁰ and $\Delta_r H^\circ(\text{FCO})$,⁵¹ we can calculate³⁶ that process (VII) should be exoergic for excitation energies above $31\,500 \pm 1000 \text{ cm}^{-1}$. Experimentally, we see fast H atoms that we attribute to secondary photodissociation of $\text{HCO}(\tilde{X})$ fragments arising *via* process (VII) at excitation wavelengths shorter than *ca.* 233 nm ($E_{\text{phot}} \approx 42\,900 \text{ cm}^{-1}$). Given that the $\text{HCO}(\tilde{X})$ fragments are expected to absorb throughout the wavelength range of interest it is very tempting to suggest that the difference in these two energies, *ca.* $11\,400 \pm 1000 \text{ cm}^{-1}$, provides a measure of the barrier height to the reverse reaction $\text{F} + \text{HCO}(\tilde{X})$, leading to electronically excited HC(O)F molecules. Whether the minimum energy pathway leads to formation of these molecules in the $\tilde{a}^3\text{A}''$ or $\tilde{A}^1\text{A}''$ state, however, is less certain. Both have the correct symmetry to correlate with ground state $\text{F} + \text{HCO}$ products, albeit after some rearrangement of the orbital occupation between these fragments and thus some mixing with higher energy configurations. Analogy with HCOOH ^{45–47} might encourage the view that this dissociation proceeds on the singlet surface, but the continued strong showing of the $\text{H} + \text{FCO}(\tilde{X})$ product channel at the shorter wavelengths, where C—F bond fission also occurs, leads us to the view that both process (VI) and (VII) occur on the $\tilde{a}^3\text{A}''$ surface after ISC as suggested in Fig. 5.

II Vibrational-energy disposal in the FCO fragments

Fig. 4 showed that the internal excitation of the FCO photofragment, $\langle E_{\text{int}} \rangle$, scales essentially linearly with increasing E_{av1} , with perhaps a hint of undulatory structure which may reflect the 'lumpy' continuum of triplet levels at energies less than and comparable to the barrier in the $\text{H} + \text{FCO}(\tilde{X})$ exit channel. This internal energy is nearly all in the form of product vibrational excitation; the rotational-energy disposal appears to be insensitive to E_{av1} . Such behaviour may be rationalised in terms of a statistical fragmentation occurring above a barrier. In what follows we build on a model for the energy disposal in such processes developed by North *et al.*⁵² and Osborn *et al.*⁵³ The key feature of such models is the assumption that the available energy $\{E_{\text{av1}} = E_{\text{phot}} - D_0[\text{HC(O)F}]\}$ divides into two separate energy reservoirs. The first of these, associated with the barrier to the back reaction (*i.e.* $E_b - D_0$ in Fig. 7) will be partitioned dynamically according to the forces acting in the transition state region. Our experiments at the longest excitation wavelengths give a good indication of the form of this energy disposal: modest *a*-axis rotational excitation of the FCO fragment, peaking at $K_a \approx 8$, with the bulk appearing as product recoil. The second reservoir, associated with the remainder of E_{av1} (*i.e.* $E_{\text{phot}} - E_b$), we assume (given the timescale of this predissociation process) to be shared out statistically. The present experiments are concerned with loss of a light H atom. Clearly, it will be necessary to consider tunnelling contributions to the total dissociation yield if we wish to model such a process quantitatively, and this constitutes the final (and novel) ingredient of the present model.

Let us consider the fragmentation of HC(O)F molecules prepared with a given $E_{\text{phot}} (> E_b)$ and, for simplicity, start by excluding the possibility of tunnelling. Following Osborn *et al.*⁵³ we recognise that each vibrational mode at the transition

state will correlate with a particular vibrational, rotational or translational degree of freedom in the products. Clearly, the C—H stretch evolves into product translation, and the two low frequency wagging motions will map into product rotation, probably contributing to the broadening of the ΔK_a distribution observed experimentally as E_{av1} increases. Without detailed knowledge of the transition state frequencies we assume the three remaining modes to have the same frequencies as in free FCO (see Table 1). This is probably least justifiable in the case of the FCO bending mode given that the calculated transition state geometry suggests an $\angle \text{FCO}$ bond angle some 6° smaller than in the ground-state radical.⁴¹ A simple statistical model would predict population of all product vibrational states with energy $E_v \leq (E_{\text{phot}} - E_b)$. For any given $\text{H} + \text{FCO}(\tilde{X}, v)$ product channel the associated translational energy arising from the statistical energy reservoir will be given by

$$E_{\text{trans}} = (E_{\text{phot}} - E_b) - E_v \quad (6)$$

and we assume that the probability for forming each of the various energetically allowed product vibrational levels scales according to the factor $(E_{\text{trans}})^{1/2}$ (*i.e.* with the available translational state density). Clearly, as Fig. 7 shows, an additional energy contribution of the order of $(E_b - D_0)$, derived from the dynamical energy reservoir, must be added to this expression for E_{trans} prior to any comparisons with the experimental TKER spectra.

Tunnelling complicates the problem in as much that it blurs the definition of E_b , and thus the demarcation between the two energy reservoirs. As Fig. 7 illustrates, a particular $\text{H} + \text{FCO}(\tilde{X}, v)$ product could arise as a result of an HC(O)F molecule tunnelling through the barrier and emerging with a substantially greater translational energy which, according to the definitions introduced in Fig. 7, we can write

$$E_{\text{trans}} = (E_{\text{phot}} - E_{\text{tun}}) - E_v \quad (7)$$

Note that this implies an expansion of the statistical energy reservoir to $(E_{\text{phot}} - E_{\text{tun}})$, with a concomitant reduction in the energy available for dynamical partitioning. Assuming an inverted parabolic barrier, the tunnelling probability (P) at an energy $(E_b - E_{\text{tun}})$ below the top of the barrier is given by

$$P(E_{\text{tun}}) = \exp[-\alpha(E_b - E_{\text{tun}})] \quad (8)$$

where α (in cm) is an attenuation coefficient, reflecting the width of the barrier. The overall probability of forming a particular $\text{FCO}(\tilde{X}, v)$ product state with vibrational energy E_v will then be given by

$$P(E_v) = \frac{\int_{D_0}^{E_b} \exp[-\alpha(E_b - E_{\text{tun}})] \{(E_{\text{phot}} - E_{\text{tun}}) - E_v\}^{1/2} dE_{\text{tun}}}{\int_{D_0}^{E_b} \exp[-\alpha(E_b - E_{\text{tun}})] dE_{\text{tun}}} \quad (9)$$

The denominator simplifies to α^{-1} , but the integral in the numerator must be evaluated numerically for each value of E_{tun} in the range $E_b \geq E_{\text{tun}} \geq D_0$, for each product vibrational level v (and associated energy E_v), and then summed.

Experiment^{32,36} provides values both for D_0 and for the energetic threshold for forming H atom photoproducts; the difference (4740 cm^{-1}) provides a lower limit to the barrier height (measured relative to the asymptotic minimum energy of the products). In an effort to further refine the magnitude of this energy barrier we have calculated internal energy spectra for a range of excitation wavelengths, with E_b and α as adjustable parameters. In each case the ultimate $P(E_{\text{int}})$ distribution required for comparison with experiment was obtained by convoluting the resulting $P(E_v)$ spectrum with a rotational distribution over the $N = K_a$ states [eqn. (4), with $K_{a(\text{max})} = 8$ and $\Delta K_a = 9$], reflecting the dynamical contribution to the

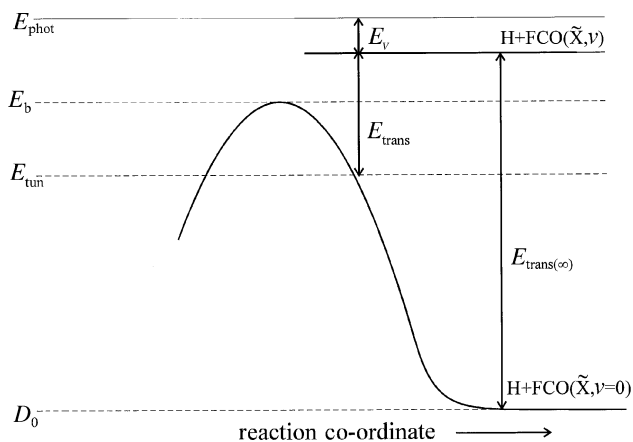


Fig. 7 Schematic illustration of the hybrid model for a statistical fragmentation occurring above a potential-energy barrier, defining the various energy terms discussed in the text

internal energy disposal. The resulting stick spectrum was then partitioned into 40 cm^{-1} wide energy bins. Comparison with the original experimental TKER spectra would require plotting $P(E_{\text{int}})$ vs. $E_{\text{trans}(\infty)}$ as defined in Fig. 7. Fig. 8 and 9 illustrate respectively, the way in which changing E_b and α influences the shape of the internal energy spectrum calculated for one particular excitation wavelength ($\lambda = 235.04 \text{ nm}$, $E_{\text{phot}} = 42\,535 \text{ cm}^{-1}$). As expected, increasing E_b (with α fixed) or increasing the attenuation coefficient α (for any chosen E_b) has the effect of truncating the higher energy part of the E_{int} spectrum. Such trial simulations do not in fact allow a precise determination of either parameter, but we judge values of $E_b = 6000 \text{ cm}^{-1}$ and $\alpha = 0.002 \text{ cm}^{-1}$ to provide the most satisfactory replication of the entire experimental data set. Fig. 10 shows the internal energy spectra these parameters would predict for the three photolysis wavelengths 246.3 nm ($E_{\text{phot}} = 40\,590 \text{ cm}^{-1}$), 239.2 nm ($E_{\text{phot}} = 41\,800 \text{ cm}^{-1}$) and 235.66 nm ($E_{\text{phot}} = 42\,420 \text{ cm}^{-1}$), each of which compares well with the

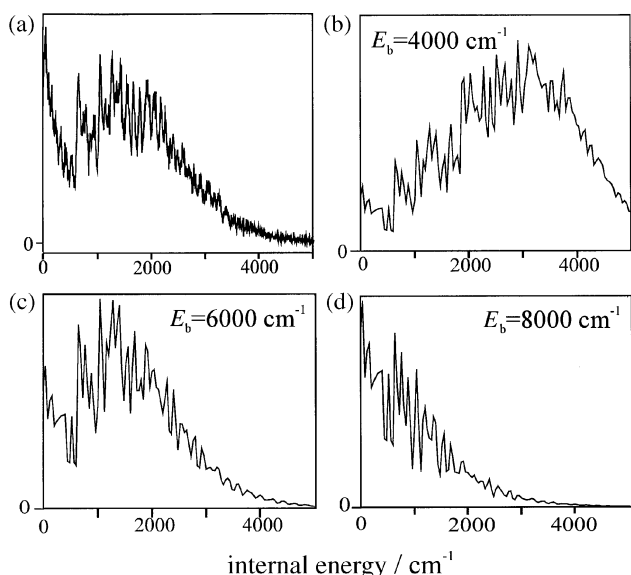


Fig. 8 Plots illustrating the way in which the the FCO internal energy disposal depends on the barrier height, E_b . (a) Experimentally derived FCO internal energy spectrum resulting from HC(O)F photolysis at 235.04 nm ($E_{\text{phot}} = 42\,535 \text{ cm}^{-1}$). (b), (c) and (d) show calculated spectra assuming the hybrid energy disposal model discussed in the text, including tunnelling, assuming $\alpha = 0.002 \text{ cm}^{-1}$ and $E_b = 4000 \text{ cm}^{-1}$, 6000 cm^{-1} and 8000 cm^{-1} , respectively. Note that the coarseness of the energy binning used in the calculation precludes precise reproduction of the rotational fine structure.

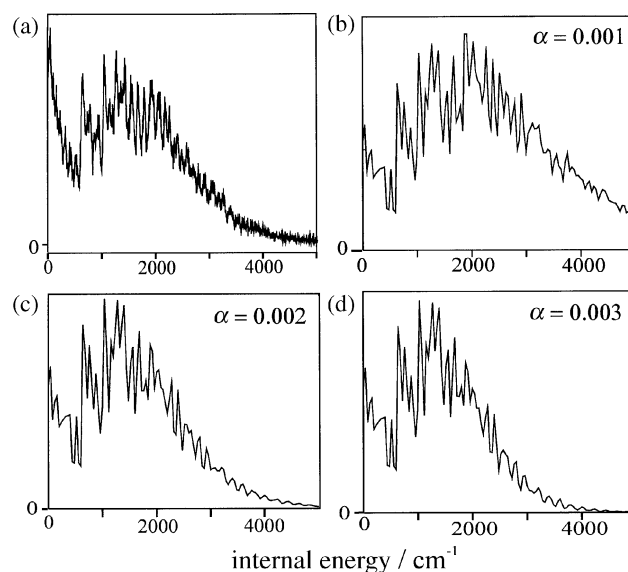


Fig. 9 Plots illustrating the way in which the the FCO internal energy disposal depends on the barrier attenuation coefficient, α . (a) Experimentally derived FCO internal energy spectrum resulting from HC(O)F photolysis at 235.04 nm ($E_{\text{phot}} = 42\,535 \text{ cm}^{-1}$), (b), (c) and (d) show calculated spectra assuming the hybrid energy disposal model discussed in the text, including tunnelling, assuming $E_b = 6000 \text{ cm}^{-1}$ and $\alpha = 0.001 \text{ cm}^{-1}$, 0.002 cm^{-1} and 0.003 cm^{-1} , respectively. As in Fig. 8, the coarseness of the energy binning used in the calculation precludes precise reproduction of the rotational fine structure.

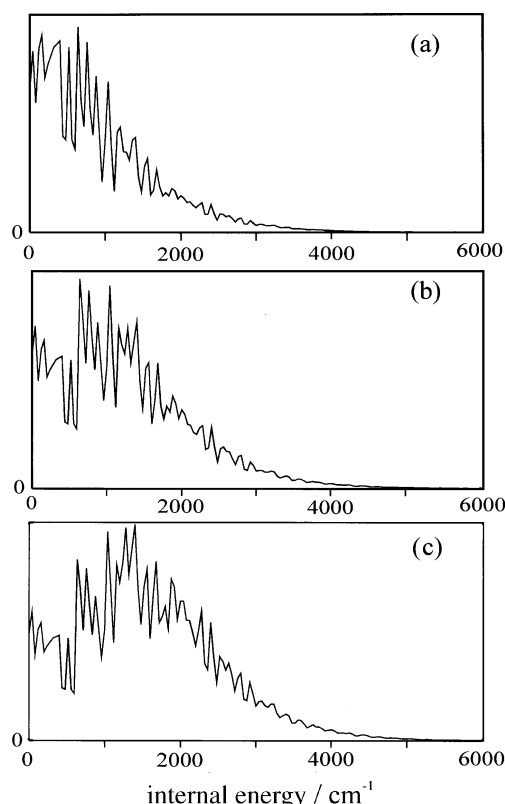


Fig. 10 FCO internal energy spectra resulting from HC(O)F photolysis as predicted by the hybrid energy disposal model described in the text assuming a barrier height $E_b = 6000 \text{ cm}^{-1}$ and an attenuation coefficient $\alpha = 0.002 \text{ cm}^{-1}$, together with photon energies of (a) $40\,590 \text{ cm}^{-1}$, (b) $41\,800 \text{ cm}^{-1}$ and (c) $42\,420 \text{ cm}^{-1}$. The overall shapes of these profiles are in good accord with the corresponding experimental E_{int} spectra displayed in Fig. 3 although, as in Fig. 8 and 9, the coarseness of the energy binning used in the calculation precludes exact reproduction of the rotational fine structure.

experimental distributions displayed previously (Fig. 3). Note, in particular, the way this model successfully accounts for the observed, near exponential, fall-off in signal at the low kinetic energy end of every experimental TKER spectrum and the absence of any fragments with recoil energies less than *ca.* 3000 cm⁻¹ (*cf.* Fig. 2).

Conclusions

The concerted programme of work described in this and the accompanying paper³⁴ has led to major advances in our understanding of the near-UV photochemistry of the prototypical carbonyl, formyl fluoride. This paper focuses particular attention on the energy disposal in the H + FCO(\tilde{X}) fragments as deduced from high resolution TOF measurements of the H atom photofragments. Spectral analysis yields a precise value for the C–H bond dissociation energy $D_0[\text{H–C(O)F}] = 34950 \pm 20 \text{ cm}^{-1}$, some 4740 cm⁻¹ less than the lowest energy at which H atom photofragments are detected in the parent ‘action’ spectrum for forming these products. This apparent discrepancy is taken as evidence for the presence of a barrier in the exit channel leading to the products H + FCO(\tilde{X}), and symmetry correlation arguments (and *ab initio* calculations^{27,28}) indicate that this barrier is part of the first excited triplet ($\tilde{a}^3\text{A}''$) potential-energy surface, accessed *via* ISC from the initially populated first excited singlet ($\tilde{A}^1\text{A}''$) state. An additional, fast, H atom peak observed at the shorter photolysis wavelengths ($\lambda < 233 \text{ nm}$) is attributed to secondary photolysis of HCO(\tilde{X}) fragments formed *via* the alternative C–F bond fission process. Symmetry and thermochemical considerations suggest that this fragmentation is also occurring on the triplet surface, and that the barrier in the F–C(O)H exit channel is *ca.* 11 400 cm⁻¹ (measured relative to the asymptotic products).

Photolysis at the longest wavelengths ($\lambda \approx 248 \text{ nm}$) results in FCO(\tilde{X}) products carrying little rotational and vibrational excitation (the former concentrated in the form of *a*-axis rotation); the bulk of the available energy [*i.e.* $E_{\text{phot}} - D_0[\text{H–C(O)F}]$] appears as product translation. The rotational-energy disposal is deduced to be almost invariant to excitation wavelength, but the extent of product vibration is found to increase near linearly with increasing E_{phot} . These observations are all explicable if the dissociation is viewed as a statistical fragmentation process occurring above a potential-energy barrier. The available energy, E_{avl} , is viewed in terms of two energy reservoirs. The first of these, corresponding to the exit channel barrier itself, is released impulsively (mainly into product translation). A simple impact parameter model assuming the calculated transition state geometry (*i.e.* the geometry at the saddle-point corresponding to the top of the exit channel barrier) suffices to reproduce the observed rotational energy disposal. The second, containing the remainder of E_{avl} , is partitioned statistically amongst the various energetically accessible vibrational states of the FCO fragment. H atom tunnelling is explicitly incorporated in the model, its inclusion serves to blur the sub-division between these two energy reservoirs, but is essential in order to obtain a good replication of all of the experimental TKER spectra.

Financial support from the EPSRC and NERC is gratefully acknowledged, as is the advice and encouragement from colleagues in Bristol (notably T. W. R. Hancock, Dr C. M. Western and K. N. Rosser) and in Bielefeld, Germany (Prof. K. H. Welge and Dr L. Schnieder). We are most grateful to Dr H. Tachikawa (Hokkaido Univ.) for communicating the results of his *ab initio* calculations of the $\tilde{a}^3\text{A}''$ surface of HC(O)F prior to publication. M. K. thanks the Japanese Society for the Promotion of Science for the award of a Post-doctoral Research Fellowship.

References

- 1 T. J. Wallington, M. D. Hurley, J. C. Ball and E. W. Kaiser, *Environ. Sci. Technol.*, 1992, **26**, 1318.
- 2 A. R. Ravishankara, A. A. Turnipseed, N. R. Jensen, S. Barrone, M. Mills, C. J. Howard and S. Solomon, *Science*, 1994, **263**, 71.
- 3 T. J. Wallington, W. F. Schneider, J. Sehested and O. J. Nielsen, *Faraday Discuss. Chem. Soc.*, 1995, **100**, 55.
- 4 S. Pinnock, K. P. Shine, T. J. Smyth, M. D. Hurley and T. J. Wallington, *J. Geophys. Res.*, 1995, **100**, 23 227.
- 5 T. J. Wallington and O. J. Nielsen, *Chem. Phys. Lett.*, 1991, **187**, 33.
- 6 A. Bhatnagar and R. Carr, *Chem. Phys. Lett.*, 1995, **238**, 9.
- 7 J. Peeters and V. Pultau, in *Proc. CEC/EUROTRAC Workshop on 'Chemical Mechanisms Describing Tropospheric Processes'*, ed. J. Peeters, Sept. 1992.
- 8 Alternative Fluorocarbon Environmental Acceptability Study, World Meteorological Organisation Global Ozone Research and Monitoring Project, Report 20, Scientific Assessment of Stratospheric Ozone, vol. 2, 1989.
- 9 *Proc. AFEAS Workshop*, Brussels, 1992.
- 10 J. Michel, H. Herrmann and R. Zellner, *Proc. EUROTRAC Symp. 1994*, ed. P. M. Borrell *et al.*, SPB Academic Publishing, Den Haag, 1994.
- 11 O. V. Rattigan, D. M. Rowley, O. Wild, R. L. Jones and R. A. Cox, *J. Photochem. Photobiol. A*, 1993, **73**, 1.
- 12 O. V. Rattigan, D. M. Rowley, O. Wild, R. L. Jones and R. A. Cox, in *Kinetics and Mechanisms for the Reactions of Halogenated Organic Compounds in the Troposphere, CEC-AFEAS Workshop*, University College Publishers, Dublin, 1993, p. 88.
- 13 T. J. Wallington, M. D. Hurley, J. M. Fracheboud, J. J. Orlando, G. S. Tyndall, J. Sehested, T. E. Møgelberg and O. J. Nielsen, *J. Phys. Chem.*, 1996, **100**, 18116.
- 14 O. V. Rattigan, D. M. Rowley, O. Wild, R. L. Jones and R. A. Cox, *J. Chem. Soc., Faraday Trans.*, 1994, **90**, 1819.
- 15 G. Bednarek, M. Briel, A. Hoffmann, J. P. Kohlmann, V. Mörs and R. Zellner, *Ber. Bunsen-Ges. Phys. Chem.*, 1996, **100**, 528.
- 16 H. W. Morgan, P. A. Staats and J. H. Goldstein, *J. Chem. Phys.*, 1955, **25**, 337.
- 17 P. Favero, A. M. Mirri and J. G. Baker, *J. Chem. Phys.*, 1956, **31**, 566.
- 18 O. LeBlanc Jr., W. W. Laurie and W. D. Gwinn, *J. Chem. Phys.*, 1960, **33**, 1960.
- 19 L. E. Giddings, Jr. and K. K. Innes, *J. Mol. Spectrosc.*, 1961, **6**, 528.
- 20 L. E. Giddings Jr. and K. K. Innes, *J. Mol. Spectrosc.*, 1962, **8**, 328.
- 21 G. Fischer, *J. Mol. Spectrosc.*, 1969, **29**, 37.
- 22 J. C. Crane, H. Nam, H. P. Beal, H. Clauberg, Y. S. Choi, C. B. Moore and J. F. Stanton, *J. Mol. Spectrosc.*, 1997, **181**, 56.
- 23 Y. S. Choi, PhD Thesis, University of California at Berkeley, 1991.
- 24 J. F. Stanton and J. Gauss, *Theor. Chim. Acta*, 1995, **91**, 267.
- 25 D. E. Klimek and M. J. Berry, *Chem. Phys. Lett.*, 1973, **20**, 141.
- 26 B. R. Weiner and R. N. Rosenfeld, *J. Phys. Chem.*, 1988, **92**, 4640.
- 27 R. Sumathi and A. K. Chandra, *Chem. Phys.*, 1992, **165**, 257.
- 28 H. Tachikawa, Hokkaido University, personal communication, 1996.
- 29 Y. S. Choi and C. B. Moore, *J. Chem. Phys.*, 1991, **94**, 5414.
- 30 Y. S. Choi and C. B. Moore, *J. Chem. Phys.*, 1992, **97**, 1010.
- 31 Y. S. Choi and C. B. Moore, *J. Chem. Phys.*, 1995, **103**, 9981.
- 32 R. N. Dixon and T. W. R. Hancock, *J. Chem. Soc. Faraday Trans.*, 1997, **93**, 2707.
- 33 T. W. R. Hancock, PhD Thesis, University of Bristol, 1997.
- 34 R. N. Dixon and T. W. R. Hancock, *J. Phys. Chem.*, in press.
- 35 G. P. Morley, I. R. Lambert, M. N. R. Ashfold, K. N. Rosser and C. M. Western, *J. Chem. Phys.*, 1992, **97**, 3157.
- 36 C. L. Reed, M. Kono, S. R. Langford, T. W. R. Hancock, R. N. Dixon and M. N. R. Ashfold, *J. Chem. Phys.*, 1997, **106**, 6198.
- 37 D. H. Mordaunt, I. R. Lambert, G. P. Morley, M. N. R. Ashfold, R. N. Dixon, C. M. Western, L. Schnieder and K. H. Welge, *J. Chem. Phys.*, 1993, **98**, 2054.
- 38 G. P. Morley, I. R. Lambert, D. H. Mordaunt, S. H. S. Wilson, M. N. R. Ashfold, R. N. Dixon and C. M. Western, *J. Chem. Soc., Faraday Trans.*, 1993, **89**, 3865.
- 39 S. H. S. Wilson, M. N. R. Ashfold and R. N. Dixon, *J. Chem. Phys.*, 1994, **101**, 7383.
- 40 G. A. Olah, M. Nojima and I. Kerekes, *Synthesis*, 1973, 487.
- 41 K. Nagai, C. Yamada, Y. Endo and E. Hirota, *J. Mol. Spectrosc.*, 1981, **90**, 249.
- 42 D. E. Milligan, M. E. Jacox, A. M. Bass, J. J. Comeford and D. E. Mann, *J. Chem. Phys.*, 1965, **42**, 3187.

- 43 S. Toby and F. S. Toby, *J. Phys. Chem.*, 1981, **85**, 4071.
- 44 R. N. Dixon, *Trans. Faraday Soc.*, 1969, **65**, 3141.
- 45 S. R. Langford, A. D. Batten, M. Kono and M. N. R. Ashfold, unpublished results.
- 46 M. Brouard, J. P. Simons and J-X. Wang, *Faraday Discuss. Chem. Soc.*, 1991, **91**, 63.
- 47 D. L. Singleton, G. Paraskevopoulos and R. S. Irwin, *J. Phys. Chem.*, 1990, **94**, 695.
- 48 Th. Krossner, L. Zülicke, R. Vetter, M. Peric and S. D. Peyerimhoff, *J. Chem. Phys.*, 1994, **101**, 3973.
- 49 Th. Krossner, M. Peric, R. Vetter and S. D. Peyerimhoff, *J. Chem. Phys.*, 1994, **101**, 3981.
- 50 M. W. Chase, Jr., C. A. Davies, J. R. Downey, Jr., D. J. Frurip, R. A. McDonald and A. Syverud, *J. Phys. Chem. Ref. Data*, 1985, **4**, suppl. 1.
- 51 T. J. Buckley, R. D. Johnson III, R. E. Huie, Z. Zhang, S. C. Kuo, and R. B. Klemm, *J. Phys. Chem.*, 1995, **99**, 4879.
- 52 S. W. North, D. A. Blank, J. D. Geletzer, C. A. Longfellow and Y. T. Lee, *J. Chem. Phys.*, 1995, **102**, 4447.
- 53 D. L. Osborn, H. Choi, D. H. Mordaunt, R. T. Bise, D. M. Neumark and C. H. Rohlfiing, *J. Chem. Phys.*, 1997, **106**, 3049.

Paper 7/01632H; Received 7th March, 1997